# CHANGES OF ACTION POTENTIAL
# SHAPE AND VELOCITY FOR
# CHANGING CORE CONDUCTOR GEOMETRY

STEVEN S. GOLDSTEIN *and* WILFRID RALL

*From the Mathematical Research Branch, National Institute of Arthritis, Metabolism, and Digestive Diseases, Bethesda, Maryland 20014*

ABSTRACT   The theoretical changes in shape and velocity of an action potential were computed in regions of changing core conductor geometry. Step decrease and step increase of diameter, branch points, and gradual taper or flare of diameter were studied. Results showed increase of both velocity and peak height as the action potential approaches a point of step decrease. A step increase causes decrease of both velocity and peak height with approach; propagation may either fail, succeed with brief delay, or, with longer delay, succeed in both forward and reverse directions. With branching, both the shape and the dimensionless velocity, $\tau\theta/\lambda$, remain unchanged when the $d^{3/2}$ values are matched. Without such matching, the changes of shape and dimensionless velocity of an action potential correspond to those found for step decrease or step increase of diameter. For regions of flare or taper, it was found (for a specific previously defined class) that velocity changed in proportion with the changing length constant. A simple formula was found to predict how this proportionality constant depends upon the amount of flare or taper.

## INTRODUCTION

Theoretical and computational studies of action potentials have usually taken advantage of one or the other of the following simplifying assumptions: either space clamping conditions are assumed to prevent action potential propagation completely, or uniform properties and infinite length are assumed to provide propagation at constant velocity. Both assumptions offer the great computational advantage of permitting the partial differential equation (cable equation for spatio-temporal spread of membrane potential disturbances) to be reduced to an ordinary differential equation.

Here, neither simplifying assumption is permissible, because we wish to focus upon changes in the shape and the velocity of an action potential as it approaches a region of changing core conductor geometry. The specific kinds of change in geometry considered are illustrated in Fig. 1; included are sealed termination, step decrease or increase of diameter, taper or flare of diameter, and branching.

Depending upon the kind and the amount of the geometric change, action potential propagation can become faster, slower, or remain the same as it approaches the region of geometric change; also, it can fail to propagate beyond this region, or it can succeed

with or without delay. Under certain conditions, it can propagate backwards as well as forwards from this region. Our purpose is to obtain information and gain biophysical understanding of such changing action potential behavior.

*Relation of Shape and Velocity*

In order to clarify the relation between action potential shape and velocity, we make use of Fig. 2. There each shape is shown as a function of distance $(x/\lambda)$, and propagation is from left to right. The upper two shapes illustrate propagation of a constant shape at constant velocity; every point, such as $A$ to $A'$ or $B$ to $B'$, travels at the same velocity. In contrast, the lower two shapes illustrate propagation of a changing shape; then it can be shown that corresponding points, such as $C$ to $C'$, and $D$ to $D'$, travel neither at the same velocity nor at a constant velocity. What is more, with changing shape, even the definition of corresponding points presents a problem. Our choice has been to treat them as corresponding fractions of the changing peak voltage of the action potential in the distance domain (where the falling phase must be distinguished from the rising phase).

For the case of constant shape, there is no difficulty in characterizing the velocity. Given a
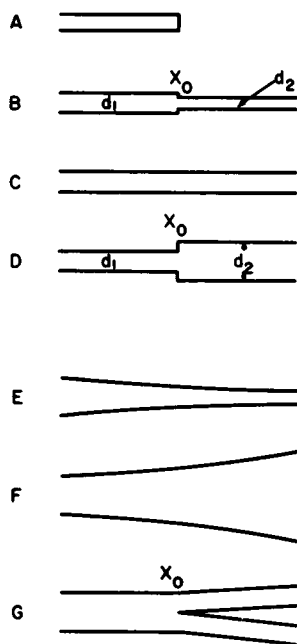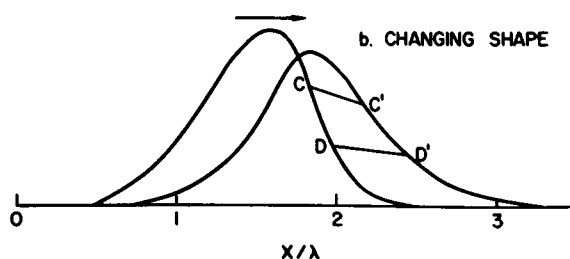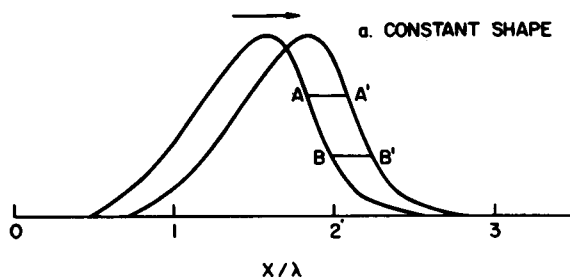


FIGURE 1



FIGURE 2

FIGURE 1    Summary of geometric regions considered, shown in longitudinal section.

FIGURE 2    Action potential propagation with constant and changing shape. The letters $A$, $B$, $C$, $D$ represent points on the action potential at a given time. The corresponding points at a later time are $A'$, $B'$, $C'$, $D'$, respectively.

time increment, d*t*, every point advances by the same distance, d*x*, such as *A* to *A'*, or *B* to *B'*; the propagation velocity, $\theta$, is then unambiguously defined as this d*x* divided by this d*t*. Thus

$$\theta = (dx)/(dt) \qquad mm/ms, \qquad (1)$$

and it can be shown that $\theta$ is not only the same for all pairs of corresponding points, but $\theta$ also remains constant as the action potential propagates to other locations along a uniform cylinder of infinite length. For such conditions it is well known that

$$\partial V/\partial t = -\theta(\partial V/\partial x), \qquad (2)$$

where *V* represents the departure of membrane potential from its resting value. This equation has several implications: the action potential shape in the time domain is proportional to the shape in the distance domain, with $-\theta$ as the constant of proportionality; the peak in the time domain occurs at the same *x* and *t* as in the distance domain.

For the case of propagation with changing shape we cannot use Eq. 1 to define a unique velocity for such an action potential, and Eq. 2 does not apply. In order to be more explicit, we consider the total differential of *V*, which is defined as

$$dV = (\partial V/\partial x)dx + (\partial V/\partial t)dt. \qquad (3)$$

For corresponding points, *A* to *A'* and *B* to *B'*, d*V* = 0, and rearrangement of Eq. 3 with substitution of Eq. 1 yields Eq. 2. But which changing shape, as for corresponding points *C* to *C'* and *D* to *D'*, d*V* $\neq$ 0, and rearrangement of Eq. 3 yields

$$\partial V/\partial t = (dV)/(dt) - (\partial V/\partial x)(dx)/(dt). \qquad (4)$$

With d*V* $\neq$0, this equation has implications that contrast with those of Eq. 2: the action potential shape in the time domain is not proportional to the shape in the distance domain; the peak in the time domain (i.e., for a given $x = x_1$, the time at which $\partial V/\partial t = 0$ can be designated $t = t_1$) does not occur at the same *x* and *t* as in the distance domain (i.e., for $t = t_1$, the location where $\partial V/\partial x = 0$ cannot be $x = x_1$); also, corresponding points in the distance domain do not agree with corresponding points in the time domain.

Because the velocity of such an action potential is not defined, we have chosen to focus attention upon the changing velocity of the peak in the time domain. This velocity can be expressed

$$\theta_p = \lim_{\Delta t \to 0} [\Delta x/\Delta t]_p, \qquad (5)$$

where it is understood that subscript *p* means that $\Delta x$ and $\Delta t$ are chosen as follows: $\partial V/\partial t = 0$ both at $x = x_1$, $t = t_1$, and at $x = x_1 + \Delta x$, $t = t_1 + \Delta t$.

In order to explore such velocity and shape changes in regions of changing geometry (Fig. 1) we simulated action potential propagation by means of a mathematical model.

The specific mathematical model used in our computations is shown below as Eqs. 10–12. This model is a particular case of a general class of models defined and discussed by FitzHugh (1969); see also Evans and Shenk (1970). Because some theoretical considerations are common to this entire class, we present it first.

### General Mathematical Model

This general model consists of the following system of partial differential equations:

$$(\partial^2 V/\partial X^2) - (\partial V/\partial T) = f(V, W_1, \ldots W_n) \qquad (6)$$

$$(\partial W_j/\partial T) = f_j(V, W_1, \ldots W_n) \qquad \text{for } j = 1, \ldots n, \qquad (7)$$

where $V$ represents the departure of the transmembrane potential from its resting value (millivolts), $W_1, \ldots W_n$ are auxiliary variables defined by Eq. 7, and both $X$ and $T$ are dimensionless variables defined as follows: $X = x/\lambda$, where $x$ is actual distance (millimeters) and $\lambda$ is the length constant[1] (millimeters); $T = t/\tau$, where $t$ is time (milliseconds), and $\tau$ is the passive membrane time constant[1] (milliseconds). Such systems have been shown to simulate propagating action potentials for suitable choice of $f$ and $f_j$. The Bonhoeffer-van der Pol model of FitzHugh (1961, 1969) includes only one auxiliary variable and one $f_j$. The model of Hodgkin and Huxley (1952) includes three auxiliary variables ($m$, $n$, and $h$).

These equations apply to propagation in a uniform cylinder. When core conductor diameter changes with distance, Eq. 6 must be replaced by a more general expression (see section on tapering diameter below) in which the definition of $X = x/\lambda$ becomes generalized (see also Rall, 1962).

*Velocity in Different Domains.* Here we restrict consideration to the propagation of a single action potential in a uniform cylinder of infinite length. As others have done, we assume for this a constant velocity, $\theta$; see Eqs. 1 and 2 above. It is well known that $\theta$ will have different values in different cylinders. Even for identical active membrane properties ($f$ and $f_j$), $\theta$ will be different for different $\lambda$ and different $\tau$; however, this particular difference disappears in the dimensionless space of $X$ and $T$, where Eq. 2 becomes transformed to

$$\partial V/\partial T = -(\tau\theta/\lambda)\partial V/\partial X. \qquad (8)$$

The dimensionless velocity, $\tau\theta/\lambda$, is the same for all cylinders (regardless of diameter, $\lambda$ or $\tau$ value) which have the same active membrane properties ($f$ and $f_j$). This assertion follows immediately from the fact that Eqs. 6 and 7 are not dependent

---

[1] $\tau$ and $\lambda$ are cable parameters defined in terms of *passive* cable properties; by definition, they remain unaffected by the permeability changes associated with active propagation.

upon the values of $\lambda$ and $\tau$; in other words, dimensionless propagation velocity in $X$, $T$ space depends only upon $f$ and $f_j$; see also FitzHugh (1973).

*Distance Domain.* When we compare constant propagation in two cylinders which differ only in their diameters, we know that both the shape and the velocity of the action potential are identical with respect to $X$, but they will be different with respect to $x$. If the two cylinders have diameters, $d_1$ and $d_2$, with characteristic lengths, $\lambda_1$ and $\lambda_2$, we know that $\tau\theta_1/\lambda_1$ equals $\tau\theta_2/\lambda_2$ and therefore, that

$$\theta_1/\theta_2 = \lambda_1/\lambda_2 = (d_1/d_2)^{1/2} \tag{9}$$

where the last expression represents the well-known dependence of $\lambda$ upon the square root of diameter. (This implies the usual assumption of extracellular isopotentiality.)

For example, if $d_1$ is $4d_2$, not only the velocity in the $x$ domain will be twice as great in cylinder 1 as in cylinder 2, but also the shape ($V$ as a function of $x$ for any particular $t$) is changed correspondingly. This is illustrated in Fig. 5, by comparing the shape at the far left (corresponding to $d_1$, $\lambda_1$, and $\theta_1$) with the more contracted shape at the far right (corresponding to $d_2$, $\lambda_2$, and $\theta_2$).[2] For any given distance (fraction of $\lambda_1$) in the left-hand shape, the corresponding distance (same fraction of $\lambda_2$) in the right-hand shape is half as great.

*Time Domain.* For two cylinders which differ only in their diameters, the action potential in the time domain has a shape ($V$ as a function of $t$ for any particular $x$) that is unchanged; in other words, different values of $\lambda$ do not change the shape in the time domain. Nevertheless, propagation velocity is still governed by Eq. 9, as long as $\tau$ has the same value in both cylinders.

### Specific Model

Simulations were performed with the following mathematical model:

$$(\partial^2 \mathcal{V}/\partial X^2) - (\partial \mathcal{V}/\partial T) = \mathcal{V} - \mathcal{E}(1 - \mathcal{V}) + \mathcal{J}(\mathcal{V} + 0.1), \tag{10}$$

$$(\partial \mathcal{E}/\partial T) = k_1\mathcal{V}^2 + k_2\mathcal{V}^4 - k_3\mathcal{E} - k_4\mathcal{J}, \tag{11}$$

$$(\partial \mathcal{J}/\partial T) = k_5\mathcal{E} + k_6\mathcal{E}\mathcal{J} - k_7\mathcal{J}. \tag{12}$$

This is a particular case of the general model defined in Eqs. 6 and 7. Here $n = 2$, $W_1 = \mathcal{E}$, $W_2 = \mathcal{J}$ and $f, f_1,$ and $f_2$ are the expressions on the right in Eqs. 10–12. Also, the variable voltage, $V$, has been replaced by a dimensionless variable, $\mathcal{V}$, which has been normalized to make $\mathcal{V}$ range from 0 to 1 as $V$ ranges from 0 to the excitatory equilibrium potential; more detail on this normalization can be found on p. 79 of Rall (1964).

---

[2] With regard to Fig. 5, it may be noted that while the shapes are distorted near the origin (where the two cylinders are joined), those farthest from the origin are essentially the same as at greater distances.

| | Kinetic parameters | | | | | | | Propagation velocities | | | |
|---|---|---|---|---|---|---|---|---|---|---|---|
| | $k_1$ | $k_2$ | $k_3$ | $k_4$ | $k_5$ | $k_6$ | $k_7$ | $\tau\theta/\lambda$ | $\theta$(Squid)* | $\theta$(Lobster)* | $\theta$(Crab)* |
| | | | | | | | | | $m/s$ | $m/s$ | $m/s$ |
| A | 1,500 | 30,000 | 25 | 0.2 | 2.4 | 0.05 | 10 | 5.0 | 36 | 6.2 | 2.5 |
| B | 500 | 30,000 | 25 | 0.2 | 7.4 | 0.05 | 15 | 4.9 | 35 | 6.1 | 2.45 |
| C | 500 | 300,000 | 25 | 0.2 | 7.4 | 0.05 | 10 | 8.0 | 57 | 10 | 4.0 |
| D | 500 | 30,000 | 25 | 0.2 | 7.4 | 0.05 | 10 | 5.0 | 36 | 6.2 | 2.5 |
| E | 63 | 3,800 | 3.1 | 0.025 | 0.95 | 0.062 | 1.3 | 3.2 | 23 | 4.0 | 1.6 |

*Values, based on experimental $\tau$ and $\lambda$ values from Katz (1966): $\lambda = 5$ mm $\quad \lambda = 2.5$ mm $\quad \lambda = 2.5$ mm $\quad \tau = 0.7$ ms $\quad \tau = 2$ ms $\quad \tau = 5$ ms

This particular model (Eqs. 10–12) was previously used to generate action potentials needed in a computational reconstruction of potentials in the olfactory bulb (Rall and Shepherd, 1968). For several different choices of $k_1, \ldots k_7$, such as those shown in Table I, we have obtained well-shaped propagating action potentials which can be re-garded as mathematically stable (see Evans, 1972). Because the values of $k_1, \ldots k_7$ remain constant (independent of $\mathcal{V}$, $X$, and $T$), computation with this system is sig-nificantly simpler than with that of Hodgkin and Huxley (1952). In Table I, each set of $k_1, \ldots k_7$ is followed by the dimensionless velocity, $\tau\theta/\lambda$, found by numerical solution for constant propagation in a uniform cylinder of infinite length. To facilitate comparison with experimental velocities, these $\tau\theta/\lambda$ values are reexpressed in Table I as particular velocities, $\theta$, for particular $\tau$ and $\lambda$ values from the literature (see Katz, 1966).

*Numerical Solutions.* The set of partial differential equations (PDE) 10–12 was solved simultaneously using standard numerical techniques. The explicit method of solution was used (see Smith, 1965). The ratio of the time step, $\Delta t$, to the square of $\Delta X$ was 0.04.

The validity of this solution was tested for the case of constant propagation in the uniform cylinder. Here, we can make use of Eq. 8 to convert the system of partial differential equations (10–12) to the following system of ordinary differential equations (ODE):

$$(d^2\mathcal{V}/dX^2) + (\tau\theta/\lambda)(d\mathcal{V}/dX) = \mathcal{V} - \mathcal{E}(1 - \mathcal{V}) + \mathcal{J}(\mathcal{V} + 0.1), \quad (13)$$

$$-(\tau\theta/\lambda)(d\mathcal{E}/dX) = k_1\mathcal{V}^2 + k_2\mathcal{V}^4 - k_3\mathcal{E} - k_4\mathcal{E}\mathcal{J}, \quad (14)$$

$$-(\tau\theta/\lambda)(d\mathcal{J}/dX) = k_5\mathcal{E} + k_6\mathcal{E}\mathcal{J} - k_7\mathcal{J}, \quad (15)$$

This system of equations explicitly contains the dimensionless velocity, $\tau\theta/\lambda$. As was found originally by Hodgkin and Huxley (1952), we also found that an action potential

solution of such a system of ODEs is extremely sensitive to a correct choice of velocity. The Runge-Kutta method of numerical solution was used. When the choice of velocity had been refined to eight significant figures, the shape of the rising phase and the peak of this action potential was found to at least three significant figures. When this solution (of Eqs. 13–15) was compared with that obtained by numerical solution of the PDEs 10–12 agreement to three significant figures was found for the rising phase and peak.

Clearly the ODEs 13–15 do not apply to regions where changing geometry causes changing shape and velocity. All such computations were necessarily made with the PDEs 10–12 (or 24–26 below). When performing such calculations, the initial condition was that $\mathcal{V} = \mathcal{E} = \mathcal{J} = 0$ for all $X$, except that a suprathreshold transmembrane potential ($\mathcal{V} = 0.9$) was imposed along a short length ($\Delta X = 0.2$) located $1.5\ \lambda$ away from the region of interest. It was verified by our computations that the resulting action potential had constant shape and velocity before entering the region of interest. In the preparation of the figures, the after hyperpolarization portion of each action potential was omitted to avoid unnecessary confusion from overlaps.

### Tapering Diameter

Here we consider noncylindrical core conductors which taper or flare continuously with distance. Such changing diameter implies a continuously changing $\lambda$. To emphasize this difference between a cylinder and a tapering core conductor we define a *generalized* length parameter, $\lambda_{\text{taper}}$, and a *generalized* electrotonic distance, $Z$, which are related to each other as follows:

$$\lambda_{\text{taper}} = \lambda_0 (r/r_0)^{1/2} [1 + (dr/dx)^2]^{-1/4}, \tag{16}$$

$$dx/dZ = \lambda_{\text{taper}}, \qquad \text{or} \quad Z_2 - Z_1 = \int_{x_1}^{x_2} (1/\lambda_{\text{taper}}) dx, \tag{17}$$

where $\lambda_0$ is the length constant for a cylinder with a radius, $r_0$, taken as the radius at a reference location. The new variable, $Z$, replaces the previously used dimensionless distance, $X = x/\lambda$. The basis for these equations can be found on pp. 1078–1079 of an earlier publication (see Rall, 1962).

Our considerations are here restricted to a *particular* class of core conductors where the amount of flare or taper is determined by a single parameter, $K$, according to Eq. 18. Examples for several values of $K$ are illustrated graphically in Fig. 11. For this class, the radius changes monotonically with distance according to the rule:

$$r^2 \propto (dx/dZ) \exp(KZ). \tag{18}$$

For some purposes it is desirable to express the dependence of $r$ upon $x$ rather than $Z$; this is provided by Eq. 22 below. Although this dependence is complicated in the most general case (see Appendix), it can be well approximated for most cases of

interest, where $(dr/dx)^2$ is much smaller than unity.[3]   When this approximation is used, we can simplify Eq. 16 and 17 to

$$dx/dZ \simeq \lambda_0(r/r_0)^{1/2}. \tag{19}$$

By substituting Eq. 19 into proportionality 18, we obtain

$$r \simeq \exp(2KZ/3), \tag{20}$$

where the proportionality constant is $r_0$.   When this $r/r_0$ is substituted into Eq. 19, integration yields

$$x/\lambda_0 \simeq (3/K)[\exp(KZ/3) - 1]. \tag{21}$$

Now substitution of $(r/r_0)^{1/2}$ for $\exp(KZ/3)$ in Eq. 21 yields an expression which can be rearranged to the following simple dependence of $r$ upon $x$

$$r/r_0 \simeq ([Kx/3\lambda_0] + 1)^2. \tag{22}$$

This also implies

$$\lambda_{taper} \simeq \lambda_0([Kx/3\lambda_0] + 1). \tag{23}$$

For the class of taper or flare defined by Eqs. 16–18, it can be shown that the earlier model Eqs. 10–12, which apply to cylinders, become generalized to the following

$$(\partial^2 \mathcal{V}/\partial Z^2) + K(\partial \mathcal{V}/\partial Z) - (\partial \mathcal{V}/\partial T) = \mathcal{V} - \mathcal{E}(1 - \mathcal{V}) + \mathcal{J}(\mathcal{V} + 0.1) \tag{24}$$

$$\partial \mathcal{E}/\partial T = k_1\mathcal{V}^2 + k_2\mathcal{V}^4 - k_3\mathcal{E} - k_4\mathcal{E}\mathcal{J} \tag{25}$$

$$\partial \mathcal{J}/\partial T = k_5\mathcal{E} + k_6\mathcal{E}\mathcal{J} - k_7\mathcal{J} \tag{26}$$

This assertion is based upon the demonstration (Rall, 1962) that $\partial^2 \mathcal{V}/\partial X^2$ for the cylindrical case becomes replaced by $\partial^2 \mathcal{V}/\partial Z^2 + K\partial \mathcal{V}/\partial Z$ for this class of taper. Also, it may be noted that the special case of zero taper, which implies $dr/dx = 0$ and $K = 0$, reduces $Z$ to $X$ and $\lambda_{taper}$ to $\lambda_0$, with the result that the more general model (Eqs. 24–26) is reduced to the cylindrical model (Eqs. 10–12).

### RESULTS

#### Case of Membrane Cylinder with Sealed End

Here we examine the changes in shape and velocity found for a computed action potential as it approaches a sealed (insulated) boundary.  By a sealed end (Fig. 1 A) we

---

[3] To verify that $dr/dx$ is sufficiently small in any given case, one can evaluate the derivative of Eq. 22 below. For example, if $K = 3$, $r_0/\lambda_0 = 0.002$ and $x/\lambda_0 = 49$, then $dr/dx = 0.2$ and the factor $[1 + (dr/dx)^2]^{-1/4} = 0.990$ in Eq. 16.
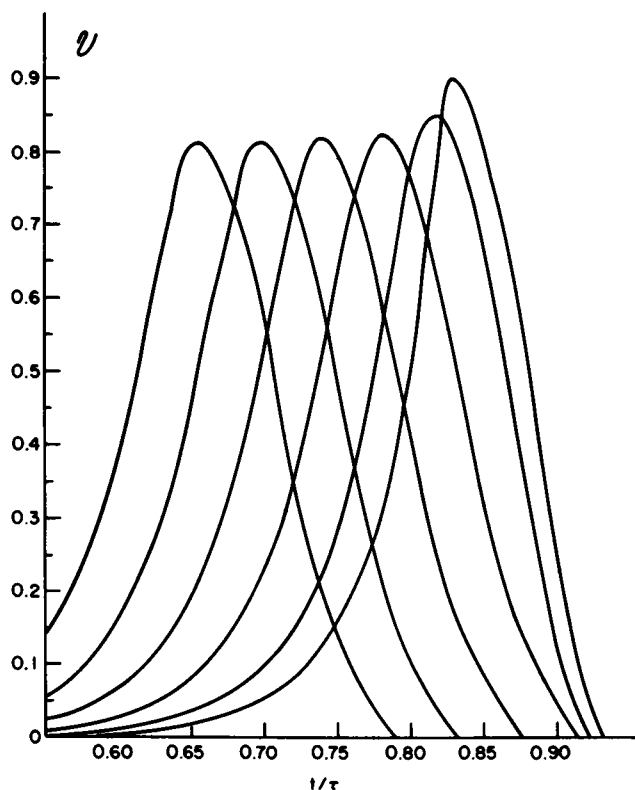
FIGURE 3 Action potential approaching a sealed end. Each shape represents the action potential (in the time domain) at six equally spaced ($\Delta X = 0.2\lambda$) locations along the cylinder. The leftmost curve corresponds to a location $X = 1$ from the sealed end.

mean that no current can leak across the membrane which closes the end of the cylinder; this corresponds to $\partial V/\partial X = 0$ at this boundary. The result, that both the peak and the velocity of the action potential increase as it approaches such a sealed boundary, is illustrated by the six curves in Fig. 3. These curves show temporal action potentials ($\mathcal{V}$ vs. $T$) at six equally spaced ($\Delta X = 0.2$) locations along the cylinder. The leftmost curve represents the action potential at a distance of $\lambda$ away from the boundary; this curve has essentially the same shape and velocity as the action potential propagating in a cylinder of infinite length. From left to right, these curves show increasing peak height, narrowing half-width, and decreasing temporal displacement, as the action potential approaches the sealed boundary. With regard to velocity, the peak displacement at left is $\Delta T = 0.04$, implying a dimensionless velocity, $\tau \theta_p/\lambda = \Delta X/\Delta T = 5.0$; in contrast, the peak displacement at right is $\Delta T = 0.01$, implying $\tau \theta_p/\lambda = 20$, a fourfold increase.

In common with our other computed results, this figure shows that significant changes in shape and velocity occur only at locations less than $\lambda$ from the boundary; the major effect occurs within $\lambda/2$.

It has been noted that when collision occurs between two action potentials propagating in opposite directions in a cylinder of infinite length, the conditions at the point of collision are equivalent to those at the sealed end (e.g., p. 467, Katz and Miledi, 1965). This is because symmetry implies $\partial V/\partial x = 0$ at the point of collision. It follows that peak height and velocity must increase just before collision and extinction.

In order to obtain biophysical understanding of such increase in peak height and velocity, we draw attention to the distribution of core current that flows downstream, ahead of the active membrane region. When the action potential is far from a boundary or point of collision, the leading core current is free to flow downstream for a considerable distance; it can leave the core over a large area of membrane at relatively low membrane current density. As the action potential approaches the point were $\partial V/\partial x = 0$, the core current cannot flow beyond this point, and must leave the core over a limited area of membrane at relatively high membrane current density. Such increased local current results in more rapid membrane depolarization, earlier attainment of threshold and peak (implying increased velocity); also the extra local current augments the amplitude of the peak.

### Case of Step Reduction of Cylindrical Diameter (Fig. 1 B)

Fig. 4 shows an example of the changes in shape of an action potential as it traverses the region near a step reduction. The wave is viewed in the time domain at points labeled $X_A$, $X_0$, and $X_B$ in the figure. Dotted curves show a reference action potential in a uniform cylinder of the initial diameter.

The behavior is qualitatively similar to the sealed end in that the peak is both earlier and higher, and the half-width is reduced as it approaches the boundary point, $X_0$. After the action potential passes $X_0$, it soon returns to its initial shape in the time domain, but its velocity becomes slower (as shown by the increased latency of the solid curve at $X_B$), as should be expected for the reduced diameter. The shape of an action potential is essentially stable when its peak is more than $X = 1$ distant from $X_0$ on either side.

*Distance Domain.* Fig. 5 shows the same action potential in the distance domain. The curves are shown at equal time intervals. One notes immediately that the wave on the extreme right is narrower than the initial wave on the extreme left. Since these waves are propagating in cylinders of differing diameter, the half-width (in this distance domain) is reduced by the factor, $\lambda_2/\lambda_1$ (see Methods section, Distance Domain); also $\theta_2$ is smaller than $\theta_1$.

*Transitional Shapes.* Fig. 5 shows that the action potential in the distance domain undergoes remarkable changes in shape at distances within $\lambda$ of $X_0$. These changes include not only the previously noted increase in peak height as it approaches $X_0$, but also complicated changes of slopes and half-widths. It is important to realize that in this transitional region, different points of the wave travel at different velocities, depending upon how near and on which side of $X_0$ they are located. The increase of velocity with approach to $X_0$ from the left is revealed both by increasing distance between peaks and by increasing half-width; the latter results from the fact that the rising
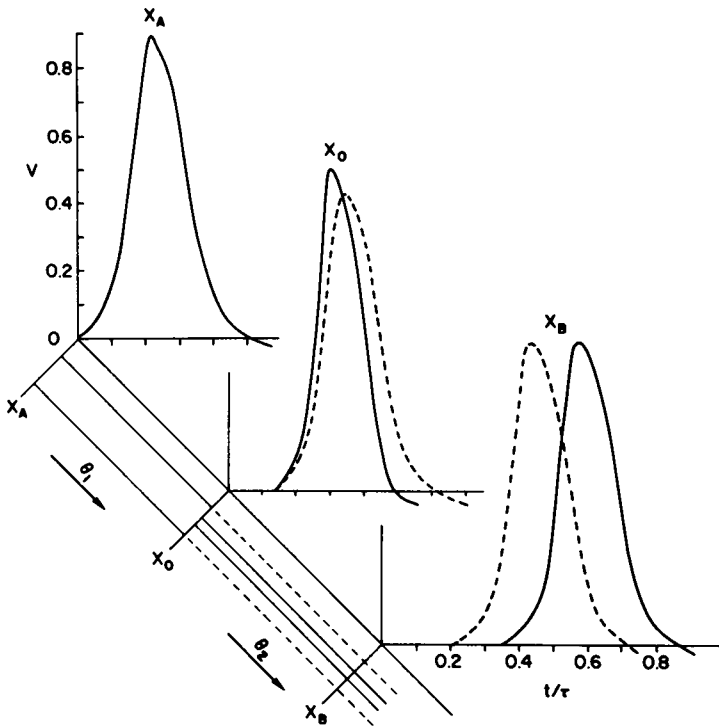
FIGURE 4   Action potential for a step reduction (at $X_0$) of cylindrical diameter. The shape (in the time domain) is shown at the points, $X_A$, $X_0$, and $X_B$. The dashed curves show the action potential as it would appear had no step reduction in diameter occurred. In this example $d_2/d_1 = 0.25$ and the kinetic parameters are shown in Table I (set A). $X_A$ and $X_B$ are $\Delta x = 0.6\lambda_1$ distant from $X_0$.
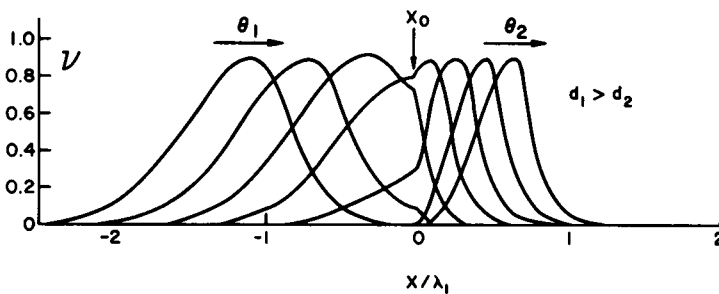


FIGURE 5   Action potential (in the distance domain) propagating in a region of step reduction (at $X_0$) of cylindrical diameter. Successive shapes from left to right illustrate the action potential at equal time intervals ($\Delta T = 0.1$). $\theta_1$ = initial constant velocity; $\theta_2$ = constant velocity attained in the smaller cylinder after passing $X_0$. In this example $d_2/d_1 = 0.25$ and the kinetic parameters are shown in Table I (set A).

phase (leading right-hand slope) is closer to $X_0$ and traveling faster than the falling phase. After passing $X_0$ (and entering the smaller diameter) decrease of velocity is revealed both by decreased distance between peaks and by decreased half-width. The contraction of the rising phase (in the distance domain to the right of $X_0$) can be understood either in terms of decreased velocity or in terms of decreased $\lambda$.

The discontinuity of slope at $X_0$ occurs because core resistance is discontinuous and continuity of current must be maintained. The core current, $I_i$, may be expressed:

$$I_i = -(\pi d_1^2/4R_i)\,[dV/dx]_{X_{0-}} = -(\pi d_2^2/4R_i)\,[dV/dx]_{X_{0+}} \tag{27}$$

where $R_i$ is the intracellular specific resistance; $X_{0-}$ and $X_{0+}$ refer to points just to the left and right of $X_0$, respectively. In the example illustrated in Figs. 4 and 5 the ratio $d_1/d_2 = 4$.

*Effect of Different Diameter Ratios upon $\theta_p$.* It is of interest to determine how velocity varies for different ratios of $d_2/d_1 \leq 1$. We will restrict attention to $\theta_p$, the velocity of the peak in the time domain. The results of simulation are shown in Fig. 6. Here the ratio $\theta_p/\theta_1$, the ratio of the changing peak velocity to the stable velocity of
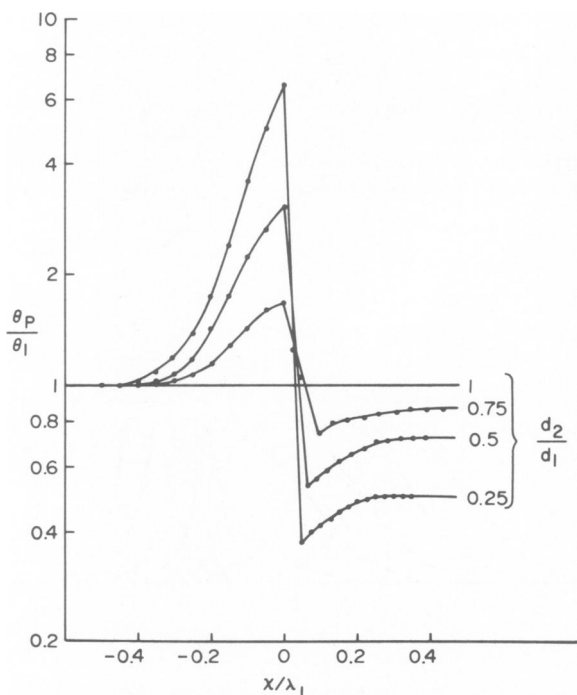
FIGURE 6  Velocity changes near a step reduction of cylindrical diameter for various diameter ratios, $d_2/d_1$. $\theta_p$, the velocity of the peak of the action potential, is normalized by $\theta_1$ the stable velocity in the initial large cylinder. The kinetic parameters are given in Table I (set B).

the initial cylinder is plotted versus distance. We note that velocity $\theta_p/\theta_1$, gradually begins to increase as the peak approaches within $x = 0.6\lambda_1$ of $x_0$; it reaches a maximum at $X_{0-}$, and falls sharply to a stable value $(\theta_2/\theta_1)$ within a distance of $x = 0.3\lambda_2$ to the right of $X_0$. As $d_2/d_1$ decreases these effects are accentuated, i.e., velocity begins to increase farther from $X_0$, rises to a greater maximum value, and falls to a lower stable value. The following empirical relation has been found to give an approximate value for $\theta_p$ at $X_0$.

$$\theta_p(X_0) \approx \theta_1(d_1/d_2)^{3/2}. \tag{28}$$

In a personal communication, Dr. John Rinzel has shown that Eq. 5 can also be expressed, $\theta_p = -\partial^2 V/\partial t^2/(\partial^2 V/\partial x \partial t)$. At $X_0$, $\partial V/\partial X$ is discontinuous and $\theta_p$ is undefined.

### Case of Step Increase of Cylindrical Diameter

Fig. 1 D illustrates the geometry of this case; here the ratio, $d_2/d_1 \geq 1$. As in the previous case, simulations were used to explore the changes in $\theta_p/\theta_1$ in the vicinity of $X_0$. In this case it was found that the velocity becomes slower as the peak approaches $X_0$. However, the effect of different $d_2/d_1$ values is more complicated than before: there are three different possibilities to be distinguished. Failure of propagation occurs when $d_2/d_1$ is large enough.[4] For smaller $d_2/d_1$, propagation continues in the larger cylinder. There is a third possibility, for intermediate $d_2/d_1$, where propagation not only continues in the larger cylinder but also reinvades the smaller cylinder, as will be explained more fully below with Fig. 10.

In Fig. 7, failure of propagation was found for $d_2/d_1 = 3.5$; the point of failure was judged to occur before the peak reached $X_0$, although a wave of subthreshold and decreasing amplitude did spread farther. Although the three curves to the left of $X_0$ in Fig. 7 show similar slowing of velocity over the range, $-0.5$ to $-0.2$ for $x/\lambda_1$, the two curves on the right show large increases of velocity. For large distance to the right of $X_0$, $\theta_p/\theta_1$ equals the stable ratio $\theta_2/\theta_1$ (i.e. Eq. 9); however, it is remarkable that $\theta_p/\theta_1$ is much larger than $\theta_2/\theta_1$ over the first quarter $\lambda$ distance to the right of $\mathring{X}$. Further details of changing velocity and wave shape in the vicinity of $X_0$ are shown below in Fig. 8 for the time domain and Fig. 9 for the distance domain. Comparable results have been reported by others: one study (Pastushenko et al., 1969 *a* and *b*) is based upon analytical treatment of a square wave action potential; the other (Khodorov et al., 1969) is based upon computations with the Hodgkin and Huxley model.

Fig. 8 shows an example $(d_2/d_1 = 2)$ of our computed action potential as it propagated through the region in question. It shows the action potential in the time domain at three points. As the wave approaches the discontinuity the peak amplitude falls,

---

[4] A familiar example is antidromic propagation of an action potential along the axon toward the axon hillock-soma region (Brock et al., 1953 Fuortes et al., 1957); this has recently been simulated by Dodge and Cooley (1973); similar antidromic propagation was also simulated in computations for mitral cells by Rall and Shepherd (1968).
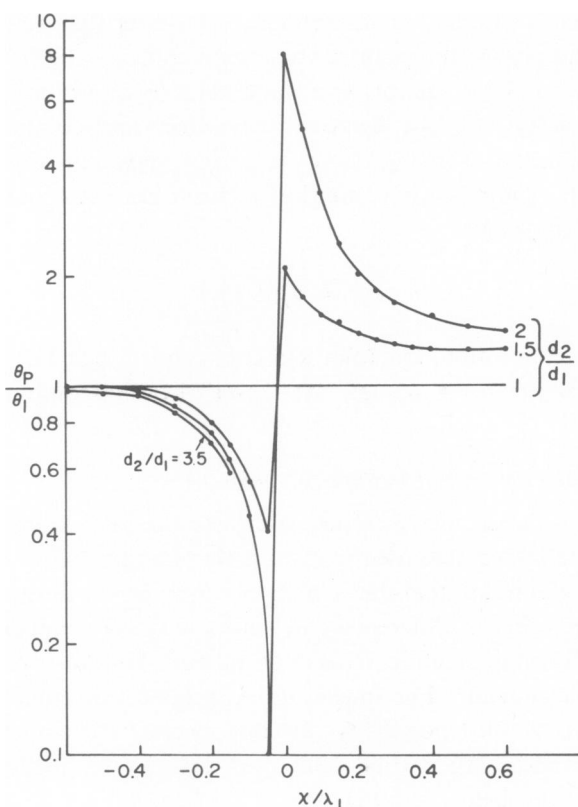
FIGURE 7 Velocity changes near a step increase of cylindrical diameter, for various diameter ratios, $d_2/d_1$. $\theta_p$, the velocity of the peak is normalized by $\theta_1$, the stable velocity in the initial small cylinder. Kinetic parameters are given in Table I (set B).

the half-width widens, and increased latency (relative to dashed control curve) reveals the slowed velocity. When the wave has reached $X_2$, the shape in the time domain has returned essentially to its original form. The increased velocity is revealed by decreasing latency (compare solid curves with dashed control curves at $X_0$ and $X_2$); in fact, the wave traveling at velocity, $\theta_2$, will shortly overtake the control (dashed) wave which travels at velocity, $\theta_1$, in the control cylinder.

*Distance Domain.* Fig. 9 shows the same action potential in the distance domain. Each wave shown is the voltage distribution along the joined cylinders at a given instant of time. The time intervals are equal. The wave on the far left has the shape it would have in an infinite cylinder of diameter $d_1$. The wave on the far right has the shape it would have in an infinite cylinder of diameter, $d_2$; it is wider by the factor $\lambda_2/\lambda_1 = 1.414$ because $d_2/d_1 = 2$ (see Eq. 9). The smaller peak amplitude at $X_0$ can be seen in Fig. 9 as well as Fig. 8.

*Transitional Shapes.* As was pointed out with Fig. 5, different points of such transitional shapes travel at different velocities; however, the changes in Fig. 9 con-
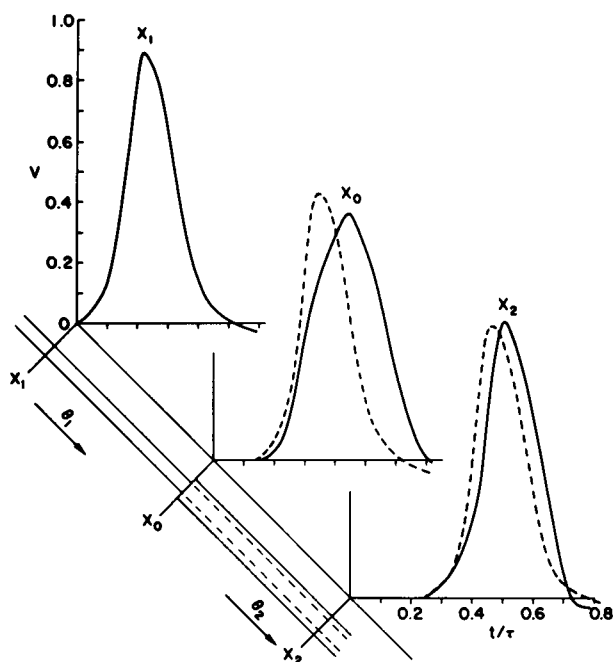
FIGURE 8 Action potential for a step increase (at $X_0$) of cylindrical diameter. The shape (in the time domain) is shown for three points $X_A$, $X_0$, and $X_B$. The dotted curves show the action potential as it would appear had no step increase in cylindrical diameter occurred. For this example $d_2/d_1 = 2.0$ and the kinetic parameters are shown in Table I (set A). $X_A$ and $X_B$ are $\Delta x = 0.6\lambda_1$ distant from $X_0$.
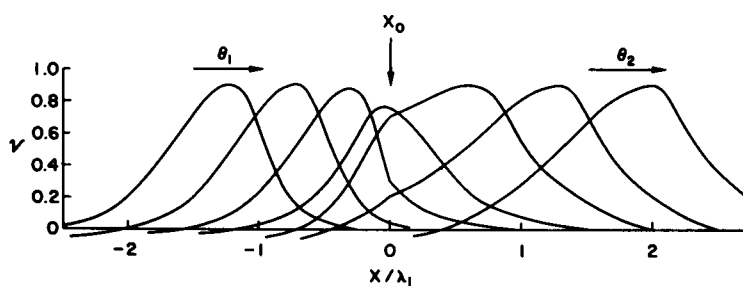


FIGURE 9 Action potential (in the distance domain) propagating in a region of step increase (at $X_0$) of cylindrical diameter. Successive shapes from left to right illustrate the action potential at equal time intervals ($\Delta T = 0.1$). $\theta_1$ = initial constant velocity; $\theta_2$ = constant velocity attained in larger cylinder after passing $X_0$. In this figure $d_2/d_1 = 2.0$ and the kinetic parameters are shown in Table I (set A).

trast with those in Fig. 5. The decrease of velocity with approach to $X_0$ from the left is revealed both by decreasing distance between peaks and by decreasing half-width; the latter results from the fact that the rising phase (leading right-hand slope) is closer to $X_0$ and traveling slower than the falling phase. After passing $X_0$ (and entering the large diameter) a large increase in velocity is revealed both by the increased peak distance and half-width of the fifth wave from the left. Although the distance between the last two peaks is not as great as this, it is still greater than that between the first two peaks; all this is consistent with the $\theta_p/\theta_1$ curve for $d_2/d_1 = 2$ in Fig. 7.

The unusual, somewhat flat-topped shape of the fifth curve from the left merits further comment. The almost flat top implies that a half $\lambda$ length of the large cylinder peaked almost simultaneously. This can be partly understood as an indirect consequence of the slowing of propagation before the peak reached $X_0$; during this slowing, there is extra time for subthreshold electrotonic spread into the larger cylinder. The resulting distribution of subthreshold voltage becomes more uniform than usual; thus both threshold and peak are reached almost simultaneously over this length (about $\lambda/2$ in Fig. 9). This near simultaneity also accounts for the high peak velocity, just to the right of $X_0$, indicated by the curve labeled $d_2/d_1 = 2$ in Fig. 7.

At $X_0$, the shapes in Fig. 9 necessarily show discontinuities in their slopes, because of the discontinuity in core resistance; see Eq. 27. Here the slopes decrease by a factor of 4.

*Forward and Reverse Propagation.* Referring back to Fig. 7, we note that $d_2/d_1 = 3.5$ resulted in failure of propagation into the larger cylinder, while $d_2/d_1 = 2.0$ resulted in success. An intermediate example, for $d_2/d_1 = 2.5$, is illustrated in Fig. 10, where voltage vs. time shapes are shown for various locations; time is displayed horizontally; spatial locations are displaced vertically; $X_0$ locates the step increase of diameter, as before. The three action potentials at far left represent propagation toward $X_0$ in the smaller cylinder. The fourth shape from the left shows the delayed action potential occurring at $X_0$. Onward propagation in the larger cylinder is shown by the nine curves labeled "forward" toward lower right. Reverse propagation in the smaller cylinder is shown by the three shapes labeled "reverse" at upper right.

To understand how reverse propagation can occur, it is useful to contrast Fig. 10 with Fig. 8, where reverse propagation did not occur. The essential difference is the longer delay in achieving an action potential at $X_0$. At the time of peak at $X_0$, the membrane of the smaller cylinder is still refractory in Fig. 8, but with the longer delay of Fig. 10, this membrane is less refractory and thus able to propagate. Partial refractoriness is evidenced by the delay of this reverse propagation.

Reverse propagation was found before in computations (Rall and Shepherd, unpublished) which simulated antidromic propagation in a mitral cell axon to its junction with the soma and dendrites. This phenomenon has also been found computationally by Zeevi (personal communication) and an example of *decremental* reverse conduction is included in his Ph.D. thesis (Zeevi, 1972). Khodorov et al. (1969) also provide an example of reverse *decremental* conduction. Both expected that such decremental
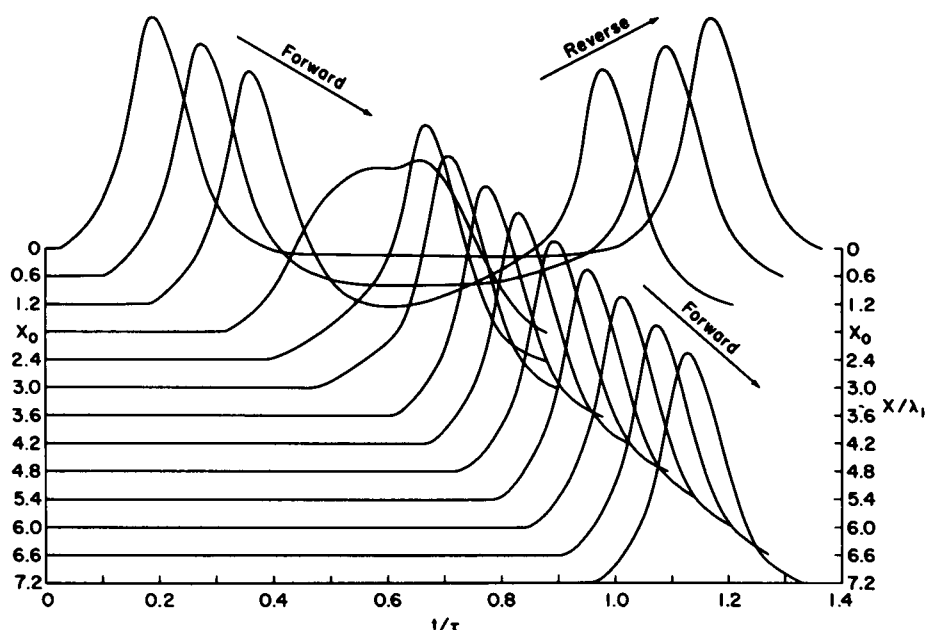
FIGURE 10  Forward and reverse propagation of the action potential in a region of step increase. The action potentials (in the time domain) are shown at successive locations indicated by the vertical scale with $X_0$ being the point of step increase. In this figure $d_2/d_1 = 2.5$; the kinetic parameters used are shown as set B in Table I.

reverse conduction might be converted to non-decremental reverse conduction if their calculations were redone with different parameters chosen to result in a shorter refractory period.

Returning to our computations with different values of $d_2/d_1$, we note that when $d_2/d_1$ is decreased from 2.5, delay in forward propagation is decreased. Thus an action potential which might propagate in reverse meets more refractory membrane. This can result in failure, i.e. reverse *decremental* conduction.

### Case of Tapering Diameter.

Computations were carried out for different degrees of taper determined by choosing several values of the parameter $K$; see Methods and Fig. 11. For any particular taper the change of $\lambda_{taper}$ with distance has already been defined by Eqs. 16–18. We expected that the velocity would also change as diameter and $\lambda_{taper}$ change with distance, and our computations verified this. What is more, we found that the velocity, $\theta$, is proportional to the changing $\lambda_{taper}$, which means that

$$\tau\theta/\lambda_{taper} = \text{constant} = \beta, \qquad (29)$$

for a given taper $(K)$ and given membrane kinetics $(k_1, \ldots k_7)$. It is noteworthy that this $\tau\theta/\lambda_{taper}$ represents a dimensionless velocity, and that its constancy means a con-
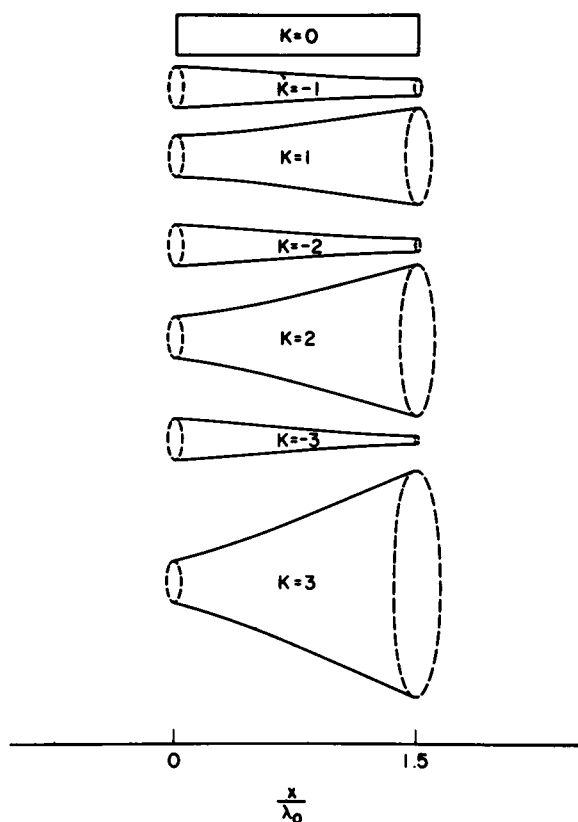
FIGURE 11 Longitudinal sections of core conductors whose radii obey the rule: $r^2 \, \alpha \, (dx/dZ) \exp (KZ)$, where $K$ is a constant and $Z$ a dimensionless distance; see also Eq. 22.

stant rate of propagation with respect to $Z$, the generalized electrotonic distance variable for taper. In addition this means that the shape of this action potential remains constant in the $Z$ domain (but changes in the $x$ domain). This also means that the shape remains constant in the time domain, as would be expected when the considerations embodied in Eq. 8 for cylinders are generalized from $X$ to $Z$. In fact, such constancy of shape in the $Z$ and $T$ domains was explicitly verified in the computed results. It is to be emphasized that these results apply only when flare or taper obeys the rule given by Eq. 18.

Because Eq. 29 implies $\theta \, \alpha \, \lambda_{taper}$ and because an earlier equation (23) shows that $\lambda_{taper}$ depends linearly upon $x$, it follows that the velocity, $\theta$, also depends linearly upon $x$, for any given $K$; that is,

$$\theta \simeq (\beta\lambda_0/\tau)(1 + Kx/3\lambda_0). \tag{30}$$

It is an interesting result of our computations with different values of $K$, that $\beta$ can be

approximated as

$$\beta \simeq (\tau \theta_c / \lambda_0) - K, \tag{31}$$

where $\theta_c$ represents the reference velocity of a cylinder ($K = 0$) with radius, $r_0$ and length constant, $\lambda_0$.

For a specific numerical illustration, we can choose a reference cylinder whose dimensionless $\tau \theta_c / \lambda_0$ value is 5. From Eq. 31, we see that $K > 5$ makes $\beta < 0$, which implies a failure of propagation; smaller values of $K$ give larger values of $\beta$. For $K = 1, 2, 3, 4$, and 4.5, the implications of Eqs. 29-31 have been plotted in Fig. 12. The intercepts at left (for $x = 0$) correspond to the value of $\beta$ for each $K$. The slope of each straight line (i.e. slope of $\tau \theta / \lambda_0$ vs. $x / \lambda_0$) is equal to $\beta K / 3$ for each $K$ value. In this
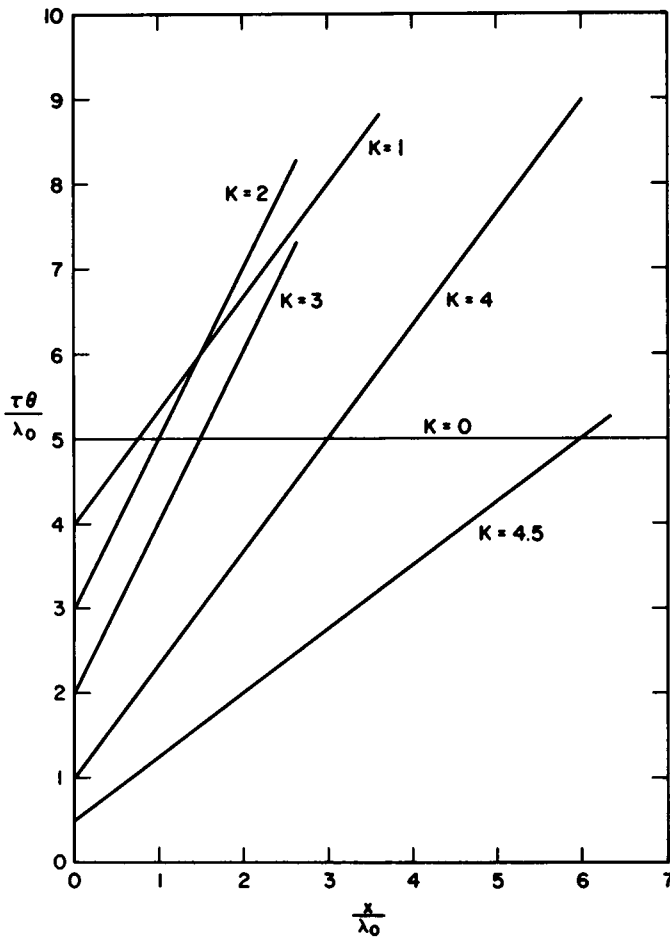


FIGURE 12  Change of velocity with distance $(x / \lambda_0)$ in flaring core conductors (with radii defined by Eq. 22). It is assumed that Eqs. 30 and 31 are valid and that $\tau \theta / \lambda_0 = 5$.

example both $K = 2$ and $K = 3$ yield slopes of 2; the steepest possible slope (2.08), corresponds to $K = 2.5$, but is not shown in Fig. 12.

It seems desirable to elaborate some of the physical intuitive meaning of the results displayed in Fig. 12. It is simplest to consider all of these core conductors as having the same diameter and $\lambda_0$ value at $x = 0$ (see Eqs. 22 and 23). Then each velocity, $\theta$, at $x = 0$, is proportional to the intercept at the left of Fig. 12. We note that increasing amounts of flare (associated with increasingly positive $K$ values) cause progressively smaller values of velocity at the point ($x = 0$) where the diameters are all the same. An explanation of this fact can be based upon the reduced core resistance that results from flaring diameter; this increases the fraction of core current that flows downstream and decreases the fraction that depolarizes adjacent membrane. Because this decreasing current must depolarize an increasing membrane capacity per unit length (because of flare), the result is less rapid membrane depolarization, implying less rapid propagation of the impulse. It may be noted parenthetically that negative $K$ values would yield increased velocity for the same core conductor diameter.

Next, we note that Fig. 12 shows that with positive $K$, the velocity in each case increases linearly with distance. At the point where each sloping line crosses the horizontal ($K = 0$) reference line, we can say that the effect of increased diameter on velocity has just compensated for the handicap associated with flare (i.e. dependence of $\beta$ upon $K$ in Eq. 31).

Referring back to Eqs. 30 and 31 we can see that flare (positive $K$) has two opposing effects on velocity in the $x$ domain: one is an increase due to increasing $\lambda_{taper}$ (see Eq. 23 in Methods), while the other is a decrease due to decreasing $\beta$ (see Eq. 31). It is these two opposing effects that explain why the slopes in Fig. 12 increase from zero, for $K = 0$, to a maximum slope for $K = 2.5$, and then decrease to smaller slopes for larger values of $K$, until $\beta$ falls to zero, implying failure of propagation.

The fact that Eq. 31 for $\beta$ is only an approximate result of the computations is made clearer by Fig. 13. Here we plot (as ordinate) the dimensionless velocity, $\tau\theta/\lambda_{taper}$, vs. $K$. It should be noted that this dimensionless velocity in the $Z$ domain is constant (independent of $x$ and core diameter) for each value of $K$. The three solid lines present results computed with three different sets of kinetic parameters, $k_1, \ldots k_7$, as made explicit by the figure legend. In each case, the dashed line is a straight line defined by Eq. 31; each dashed line was chosen by setting $\tau\theta_c/\lambda_0$ in Eq. 31 equal to $\tau\theta/\lambda_{taper}$ of each solid curve at $K = 0$. In the case of the upper solid curve, the approximate relation provides an excellent fit for dimensionless velocities greater than 3. As $K$ is increased from 4 to 6, the velocity deviates below the approximate values of the dashed line, and propagation of the computed action potential actually fails for $K = 6$, while the dashed line would imply failure for $K = 8$. This deviation can be seen to occur where the safety factor for propagation is low. Inspection of the computed results shows that the peak height of the action potential becomes significantly reduced over this range. It may be noted that this peak height decreased by only about 1% over the range ($\tau\theta/\lambda_{taper}$ from 10 to 3) where the solid line deviates negligibly from the dashed line.
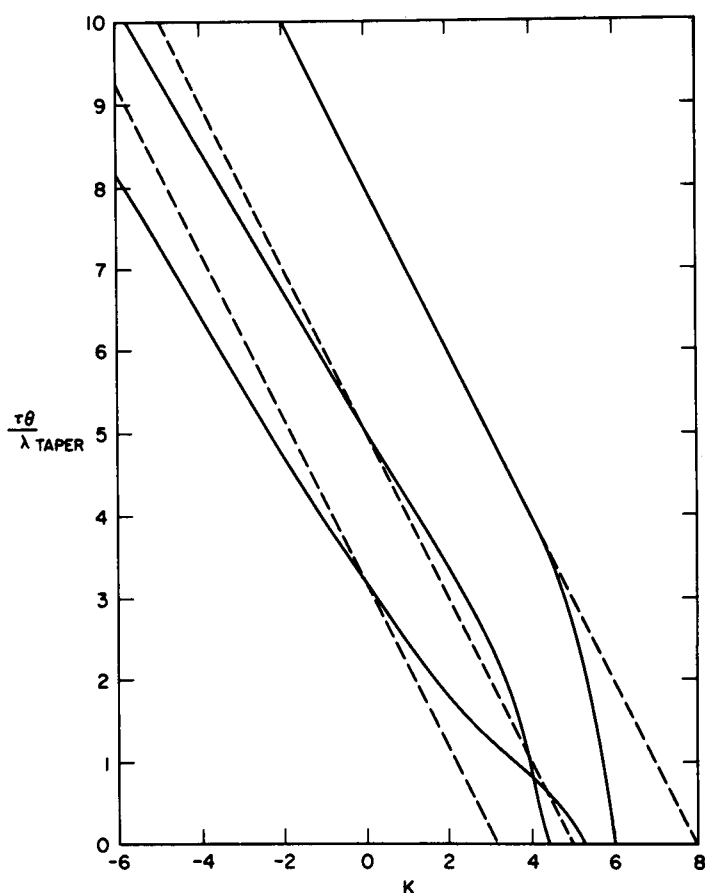
FIGURE 13 Change in dimensionless velocity, $\tau\theta/\lambda_{taper}$ with differing amounts of taper or flare. Kinetic parameters for the three solid curves shown are in Table I; the uppermost curve used set C; middle curve used set D; lowermost curve used set E.

Next we consider the deviation of the middle solid curve from its corresponding dashed straight line. For most of the dimensionless velocity range (10 to 2), there is a noticeable difference in slope, in contrast with the previous (upper) curve. This correlates well with the fact that the peak heights of the computed action potentials decreased from 0.88 to 0.75 as $\tau\theta/\lambda_{taper}$ decreases from 10 to 2. This change of peak height (approximately 15%) is much larger than that found with the upper curve. This result supports the conjecture that the dashed line represents a limiting case where action potential peak height remains unchanged. In fact, it can be demonstrated mathematically that the artificial assumption of a constant action potential shape (in the $Z$ and $T$ domains) would imply that Eq. 31 and the dashed straight lines follow exactly (see Appendix, Eqs. 37–42). The deviation of the lowermost solid curve from its corresponding dashed line also correlates with decreasing peak height: for the ve-

locity range ($\tau\theta/\lambda_{taper}$ from 8 to 2) the peak height decreases from 0.96 to 0.90, or about 6%.

At low velocities, near the point of failure, all three curves deviated from their corresponding dashed lines. The lower solid curve differs from the others in being less steep and bending more gradually as $K$ is increased toward failure. In fact, the fall is so gradual that it crosses the middle solid curve at $K = 4$. This result emphasizes the complex nature of the interaction of the active properties with the geometric properties of a core conductor at slow velocities. (It may be noted (see Table I) that the kinetic parameters corresponding to the lower curve are entirely different from the other sets. The kinetic parameters of the upper and middle curves differ only by one parameter, $k_2$).

### Branching

Computations were used to explore the effects of core conductor branching upon action potential propagation. The assumption of extracellular isopotentiality insures that the angles between the branches can be neglected.

At a branch point, it is usual to distinguish anatomically between a parent branch and a pair of daughter branches, all of which may have different diameters. However, since we wish to consider action potential propagation in either direction in any branch, it becomes necessary to adopt additional branch designations. These distinguish between that branch along which the action potential *approaches* the branch point (regardless of whether this happens to be a parent or a daughter branch), and the *other* branches (along which no action potential approaches the common branch point). Propagation behavior near the branch point depends upon the value of the geometric ratio,

$$GR = \sum_j d_j^{3/2}/d_a^{3/2}, \tag{32}$$

where $d_a$ represents the diameter of the branch along which propagation *approaches* the branch point, $d_j$ represents the diameter of the $j$th *other* branch, and the summation is over all of these *other* branches. It may be helpful to note that this geometric ratio also equals the input conductance ratio (*other* branches/*approaching* branch) for branches of semi-infinite length.

For most of our computations, we assumed all branches to be at least several $\lambda$ in length, with the result that propagation near the branch point, $X_0$, was not modified by any terminal or branching boundary conditions elsewhere. Then, the results were found to be clearly separable into three cases, determined by whether this geometric ratio, GR, is less than, equal to, or greater than unity.

*Case of GR = 1.* This case corresponds to the branching constraint (constancy of $\Sigma d^{3/2}$) which has been emphasized elsewhere (Rall, 1959, 1962, 1964) as permitting a dendritic tree to be transformed into an equivalent cylinder, for considerations of passive membrane electrotonus. Here, the *other* branches, together,

correspond to an equivalent cylinder that has the same diameter as the *approaching* branch. This means that the partial differential equation in dimensionless $X$ and $T$ applies to a continuous equivalent cylinder region that extends in both directions (upstream and downstream) from the point $X_0$.

For active propagation, it should be noted that as long as the active membrane properties are the same per unit area in all branches (i.e. independent of $\lambda$) it can be shown that the shape and velocity of the propagating action potential (in the $X$ and $T$ domains) remain constant near $X_0$; a formal demonstration can be provided by the dimensional analysis considerations of FitzHugh (1973). This expectation was verified by computations with the $\mathcal{U} \,\&\, \mathcal{J}$ model and a pair of *other* branches (of unequal diameter) satisfying GR = 1. It should be added that with propagation into these *other* branches, the shape and velocity in the $x$ domain of each branch change in proportion with each $\lambda$ value, even though both remain unchanged in the $X$ domain.

*Case of GR < 1.* Here, the *other* branches, together, correspond to an equivalent cylinder whose diameter is smaller than that of the *approaching* branch. Thus, the action potential shape and velocity in the $X$ and $T$ domains would be expected to undergo changes near the branch point, $X_0$, like those reported above for a step reduction of diameter (Figs. 4–6). Computations verified this expectation that the velocity and the peak amplitude both increase with approach to $X_0$. Also, in the *other* branches, the action potential shape and velocity soon return to their original values in the $X$ domain, but, of course to changed values in their separate $x$ domains.

*Case of GR > 1.* Here, the *other* branches, together, correspond to an equivalent cylinder whose diameter is larger than that of the *approaching* branch. We expected and we found changes near the branch point, $X_0$, like those reported above for a step increase of diameter (Figs. 7–10). Thus, the velocity and the peak amplitude both decrease with approach to $X_0$. When GR was made sufficiently large, propagation failed at $X_0$. Also, when GR was adjusted for propagation to succeed only after significant temporal delay at $X_0$, then, as in previous Fig. 10, there was retrograde propagation in the branch along which the impulse originally approached $X_0$, as well as onward propagation in all of the *other* branches. In none of these computations was propagation preferential between the *other* branches, i.e. it did not fail in one while succeeding in the others.

## DISCUSSION

Additional implications of these results should be mentioned for the closely related cases of step diameter increase and of branching with GR > 1 (see Eq. 32). In situations when failure of propagation occurs at $X_0$, there is a short time during which the residual depolarization near $X_0$ may prevent failure of a second impulse. Consequently, at different repetition rates, every second, third, or fourth impulse could succeed in propagating past $X_0$. Thus geometry alone could filter the impulse repetition rate; in the application to branching, this filtering would be the same in all of the other branches.

In the situation where propagation succeeds at $X_0$ with sufficient delay to permit retrograde propagation, it should be noted that the retrograde impulse will collide with and thus extinguish a subsequent impulse that may approach $X_0$ at this time. Since collision could occur at any point along the approaching line, the timing of the second impulse would be less critical than in the previous example.

An interesting possibility arises when a long core conductor ends in enlargements at both ends (i.e. either a step increase in diameter or branches with GR > 1). Then under favorable conditions, successive retrograde propagations could be sustained (back and forth) between these two end regions. This possibility represents another design for a pacemaker, but we have not explored this further.

Next we consider two action potentials, one in each of two branches, both approaching $X_0$ simultaneously. All the previous considerations of failure or success at $X_0$ apply here, provided that $d_a^{3/2}$ in Eq. 32 is replaced by the sum of the $d^{3/2}$ values of these two ("*approaching*") branches.

When two action potentials, one in each of two branches, are not simultaneous in their approach to $X_0$, several possibilities arise; these have been explored computationally. If the action potential in the first branch is able to propagate onward into all other branches before the action potential in the second branch reaches $X_0$, a collision of the two action potentials will occur in this second branch. If the first action potential is not able to propagate onward into the other branches, subthreshold current would spread in them passively. This would depolarize the membrane and result in an increasing velocity of the second action potential as it approaches $X_0$. A similar phenomenon has been noted independently by Pastushenko et al. (1969 *a* and *b*) using a square wave to simulate the action potential. We also observed that the possibility of retrograde conduction in the first branch is enhanced when the two waves do not reach $X_0$ simultaneously.

*Preferential Propagation into Different Branches.* The concept that preferential effects between large and small branches could contribute significant filtering of information in neural circuits has been advanced by several people; Lettvin presented this idea in several seminars and papers (Chung et al., 1970); additional references are given by Waxman (1972), and by Grossman et al. (1973). First, we emphasize that our computational and theoretical results provide no basis for such preferential effects. Then we note that this can be attributed to our simplifying assumptions: uniform membrane properties (both passive and active), extracellular isopotentiality, constant intracellular resistivity, implicitly constant ionic membrane equilibrium potentials. For example, if one were to assume that one branch is composed of more excitable membrane than the other, preferential effects could be expected. The recognition that some such additional factor is needed to explain preferential effects has been noted also by Zeevi (1972) and Grossman et al. (1973).

### APPENDIX

Here we wish to examine the consequences of changing the taper rule to lesser and greater degrees of taper. We replace our earlier Eq. 22 by a more general expression

$$r/r_0 = \left(\frac{Kx}{3\lambda_0} + 1\right)^m \tag{33}$$

where $m = 0$ corresponds to a cylinder, $m = 1$ corresponds to a conical flare or taper, $m = 2$ corresponds to our special class, and $m > 2$ corresponds to flare or taper of higher degree.

Referring back to the general treatment of taper and branching (Rall, 1962, Eq. 20) we find that the coefficient of $\partial \mathcal{V}/\partial Z$ in the general partial differential equation can be expressed

$$\text{Coef} = (dx/dZ)(d/dx)\ln[r^{3/2}n(1 + (dr/dx)^2)]. \tag{34}$$

It is this coefficient which was shown to reduce to $K$ for our special class. We set $n = 1$, because we are not here concerned with branching. Also, we restrict consideration to regions where $(dr/dx)^2$ is negligible[3] compared with unity; then Eq. 34 can be simplified to yield the approximate expression

$$\text{Coef} \simeq (3\lambda_0/2r_0)\left(\frac{r}{r_0}\right)^{-1/2}(dr/dx). \tag{35}$$

When Eq. 33 and its derivative with respect to $x$ are substituted into Eq. 35, the result is

$$\text{Coef} \simeq \frac{mK}{2}\left(1 + \frac{Kx}{3\lambda_0}\right)^{(m-2)/2} \tag{36}$$

Now, when $m = 0$, this coefficient of $\partial V/\partial Z$ is zero, and the PDE reduces to the case of a cylinder, as expected. When $m = 2$, the exponent, $(m - 2)/2$, becomes zero, and the coefficient of $\partial V/\partial Z$ reduces simply to $K$, as in Eq. 24 and in the original presentation (Rall, 1962). However, now we can use Eq. 36 to learn the consequences of different taper classes obtained by setting $m = 1$ and $m > 2$.

For conical flare, $m = 1$, and the value of Eq. 36 becomes

$$\frac{K}{2}\left(1 + \frac{Kx}{3\lambda_0}\right)^{-1/2}$$

which equals $K/2$ at $x = 0$ and decreases with increasing $x$, when $K$ is positive. As explained below, this would be expected to result in increasing dimensionless velocity, $\tau\theta/\lambda_{taper}$, with increasing $x$ and positive $K$.

For greater degrees of flare, $m > 2$, it can be seen in Eq. 36 that the exponent is positive, which means that the coefficient of $\partial V/\partial Z$ increases with increasing $x$ when $K$ is positive. As explained below, this corresponds to decreasing dimensionless velocity, $\tau\theta/\lambda_{taper}$, with increasing $x$ and positive $K$.

To understand the effect of this coefficient upon dimensionless velocity, we consider first our special class of taper which was found to result in constant dimensionless velocity, $\tau\theta/\lambda_{taper}$. For this class, we have the relation

$$\partial \mathcal{V}/\partial T = -(\tau\theta/\lambda_{taper})(\partial \mathcal{V}/dZ) \tag{37}$$

in analogy with Eq. 8 for cylinders. When this relation is substituted into Eqs. 24–26 we obtain

the following

$$(\partial^2 \mathcal{V}/\partial Z^2) + (K + \tau\theta/\lambda_{\text{taper}})(\partial \mathcal{V}/\partial Z) = \mathcal{V} - \mathcal{E}(1 - \mathcal{V})$$
$$+ \mathcal{J}(\mathcal{V} + 0.1), \quad (38)$$

$$-\tau\theta/\lambda_{\text{taper}}(\partial \mathcal{E}/\partial Z) = k_1 \mathcal{V}^2 + k_2 \mathcal{V}^4 - k_3 \mathcal{E} - k_4 \mathcal{E}\mathcal{J}, \quad (39)$$

$$-\tau\theta/\lambda_{\text{taper}}(\partial \mathcal{J}/\partial Z) = k_5 \mathcal{E} + k_6 \mathcal{E}\mathcal{J} - k_7 \mathcal{J}. \quad (40)$$

When we compare Eqs. 38–40 with the case of constant propagation in a cylinder (Eqs. 13–15), we note that the equations are quite similar. If the coefficients of $\partial \mathcal{V}/\partial Z$, $\partial \mathcal{E}/\partial Z$, and $\partial \mathcal{J}/\partial Z$ were all the same, the equations would be identical (assuming $X$ replaced by $Z$) and the action potential shapes (in the time domain) would be identical. In particular, comparison of Eq. 38 with Eq. 13 suggests that one might expect the dimensionless velocity, $\tau\theta/\lambda$ in the cylinder, to correspond to the quantity, $K + \tau\theta/\lambda_{\text{taper}}$ in the taper; this suggests

$$\tau\theta/\lambda_{\text{taper}} = \tau\theta_c/\lambda_0 - K, \quad (41)$$

which agrees with Eq. 31, where $\beta = \tau\theta/\lambda_{\text{taper}}$. Our computations showed that this relation holds approximately (see discussion of Fig. 13). To understand why this relation is not exact (theoretically) we note the fact that the coefficients of $\partial \mathcal{E}/\partial Z$ and $\partial \mathcal{J}/\partial Z$ in Eqs. 39 and 40 differ from the coefficient of $\partial \mathcal{V}/\partial Z$ in Eq. 38, whereas the corresponding coefficients in Eqs. 13–15 are identical. Nevertheless, it can be appreciated, intuitively, that departures from Eq. 41 are least when the shape of the action potential in the time domain differs negligibly between the case of a cylinder and our special class of taper.

With different classes of taper, we do not expect constant dimensionless velocity. Nevertheless, in analogy with Eq. 41, we expect that the changing velocity can be at least roughly approximated by

$$\beta = \tau\theta/\lambda_{\text{taper}} \simeq \tau\theta_c/\lambda_0 - \frac{mK}{2}\left(1 + \frac{Kx}{3\lambda_0}\right)^{(m-2)/2} \quad (42)$$

where the coefficient, $K$ in Eq. 41 has been replaced by the more general coefficient from Eq. 36. This relation implies that for the greater degrees of flare ($m > 2$, with positive $K$), the dimensionless velocity will decrease with increasing $x$. Also, for the lower degrees of flare ($m < 2$, with positive $K$), the dimensionless velocity would be expected to increase with increasing $x$. Only our special class of taper ($m = 2$), and the cylindrical case ($m = 0$) can be expected to have constant dimensionless velocity in the $Z$ domain.

## REFERENCES

BROCK, L. G., J. S. COOMBS, and J. C. ECCLES. 1953. *J. Physiol.* 122:429.
CHUNG, S., S. A. RAYMOND, and J. Y. LETTVIN. 1970. *Brain Behav. Evol.* 3:72.
DODGE, F. A., JR., and J. W. COOLEY. 1973. *IBM J. Res. Dev.* 17:219.

EVANS, J. W. 1972. *Indiana Univ. Math. J.* **22**:577.

EVANS, J. W., and N. SHENK. 1970. *Biophys. J.* **10**:1090.

FITZHUGH, R. 1961. *Biophys. J.* **1**:445.

FITZHUGH, R. 1969. *In* Biological Engineering. H. P. Schwan, editor. McGraw-Hill Book Company, New York. 1–85.

FITZHUGH, R. 1973. *J. Theor. Biol.* **40**:517.

FUORTES, M. G. F., K. FRANK, and M. C. BECKER. 1957. *J. Gen. Physiol.* **40**:735.

GROSSMAN, Y., M. E. SPIRA, and I. PARNAS. 1973. *Brain Res.* **64**:379.

HODGKIN, A. L., and R. F. HUXLEY. 1952. *J. Physiol. (Lond.)* **117**:500.

KATZ, B. 1966. Nerve, Muscle, and Synapse. McGraw-Hill Book Company, New York.

KATZ, B., and R. MILEDI. 1965. *Proc. Ry. Soc. Lond. B. Biol. Sci.* **161**:453.

KHODOROV, B. I., Y. N. TIMIN, Y. VILENKIN, and F. B. GUL'KO. 1969. *Biofizika.* **14**:304.

PASTUSHENKO, U. F., V. S. MARKIN, and Y. A. CHIZMADAHEV. 1969 *a. Biofizika.* **14**:883.

PASTUSHENKO, U. F., V. S. MARKIN, and Y. A. CHIZMADAHEV. 1969 *b. Biofizika.* **14**:1072.

RALL, W. 1959. *Exp. Neurol.* **1**:491.

RALL, W. 1962. *Ann. N. Y. Acad. Sci.* **96**:1071.

RALL, W. 1964. *In* Neural Theory and Modeling. R. F. Reiss, editor. Stanford University Press, Stanford, Calif. 73–97.

RALL, W., and G. M. SHEPHERD. 1968. *J. Neurophysiol.* **31**:884.

SMITH, G. D. 1965. Numerical Solutions of Partial Differential Equations. Oxford University Press, London.

WAXMAN, S. G. 1972. *Brain Res.* **47**:269.

ZEEVI, Y. Y. 1972. Ph.D. Thesis, University of California, Berkeley.